Ⓔ

A MULTIVARIATE ANALYSIS OF GALAXIES IN THE HUBBLE DEEP FIELD–NORTH

MICHAEL R. CORBIN, ANDREA URBAN, ELIZABETH STOBIE, RODGER I. THOMPSON, AND GLENN SCHNEIDER

NICMOS Group, Steward Observatory, The University of Arizona, Tucson, AZ 85721; mcorbin@as.arizona.edu

ABSTRACT

We use the ultraviolet and optical WFPC2 and near-infrared NICMOS images of the Hubble Deep Field–North to measure and statistically compare an array of parameters for over 250 of the galaxies it contains. These parameters include redshift, rest-frame visible asymmetry and concentration, bolometric luminosity, and extinction-corrected star formation rate. We find only one strong correlation, between bolometric luminosity and star formation rate, from which early-type galaxies noticeably deviate. When our asymmetry measurements are combined with those of a sample of nearby galaxies covering the full Hubble sequence, we find a weak correlation between redshift and rest-frame visible asymmetry, consistent with the qualitative evidence of galaxy morphological evolution from these and other deep *Hubble Space Telescope* images. The mean values of these asymmetry measurements show a monotonic increase with redshift interval over the range $0 \lesssim z \lesssim 2$, increasing by a factor of approximately 3. If this trend is real, it suggests that galaxy morphological evolution within the last $\sim 70\%$ of the Hubble time is a *gradual* process that is continuing through the present cosmological epoch. There is evidence that the dominant source of this evolution is the "minor" mergers of disk galaxies with smaller companions, which could also transform late-type spiral galaxies to early-type spiral galaxies. Interestingly, in contrast to local galaxies we find no correlations between galaxy star formation rate and either UV or visible asymmetry. This could arise if the star formation of high-redshift galaxies proceeds in episodes that are short (~ 100 Myr) relative to the timescales over which galaxy mergers produce strong asymmetries (~ 500 Myr), a result suggested by the high star formation rates of Lyman break galaxies.

Subject headings: cosmology: observations — galaxies: evolution — galaxies: fundamental parameters — galaxies: structure

On-line material: machine-readable table

1. INTRODUCTION

A major achievement of the *Hubble Space Telescope* (*HST*) has been the discovery that galaxies at intermediate and high redshift are often interacting, paired, or otherwise morphologically peculiar (see, e.g., Burkey et al. 1994; Glazebrook et al. 1995; Abraham et al. 1996a, 1996b; Driver et al. 1998; Im et al. 1999; van Dokkum et al. 1999; van den Bergh et al. 2000). Concern that this apparent peculiarity is the result of viewing galaxies above $z \sim 1$ in the rest-frame ultraviolet, in which their emission is dominated by clusters of OB stars, has largely been alleviated by images from the near-infrared camera and multiobject spectrometer (NICMOS) instrument, which provide a "morphological *K*-correction" for galaxies above such redshifts by covering their rest-frame visible emission. NICMOS images of the Hubble Deep Field–North (HDF-N), in combination with the visible images obtained by the Wide Field Planetary Camera 2 (WFPC2), have revealed a generally good (but not uniform) correspondence between the morphologies of $z \gtrsim 1$ galaxies in rest-frame ultraviolet and visible portions of their continua (Bunker 1999; Dickinson 1999, hereafter D99). Corbin et al. (2000b) also find a larger fraction of peculiar/interacting galaxies at intermediate redshift in the NICMOS parallel fields than is observed in the local universe. In addition to this increase in morphological peculiarity with redshift, there is evidence of a concurrent increase in the fraction of photometric and kinematic galaxy pairs (e.g., Neuschaefer et al. 1997; Le Fèvre et al. 2000). These results present strong evidence that galaxies have undergone significant structural evolution within the last approximately two-thirds of the Hubble time, an evolu-

tion in which merging appears to play a key role, and generally support hierarchical models of galaxy formation (e.g., Baugh et al. 1998; Kaufmann et al. 1999).

Galaxy star formation rates also show a strong increase with redshift, at least to $z \cong 1.5$ (e.g., Madau, Pozzetti, & Dickinson 1998; Thompson, Weymann, & Storrie-Lombardi 2001, hereafter TWSL01). While the form of this evolution above $z \cong 1.5$ remains highly uncertain because of the role of dust obscuration and selection effects (see TWSL01 and references therein), it apparently proceeds concurrently with the aforementioned morphological evolution. Similarly, this morphological evolution should at some level be accompanied by an evolution in galaxy luminosity and size. However, the aforementioned studies have generally concentrated on the change in only one of these quantities with redshift, rather than investigating their interrelationships. Galaxy morphological evolution has also not been properly quantified: the existing evidence of it is based on qualitative and subjective classifications of the galaxies in the HDF-N and other deep *HST* images (e.g., Im et al. 1999; van den Bergh et al. 2000). Abraham et al. (1996a) attempt such a quantification using measurements of the asymmetries and concentrations of HDF-N galaxies in the *I*-band image, but their results are limited by the lack of redshifts available for the objects at the time of their study and by the associated lack of a morphological *K*-correction provided by NICMOS images for the $z \gtrsim 1$ galaxies in the field.

These issues have motivated us to perform a statistical analysis of the galaxies in the HDF-N involving all the potentially correlated parameters and in particular to

attempt to quantify their morphological evolution. The NICMOS images of the HDF-N importantly extend the coverage of the rest-frame visible emission of its galaxies to $z \sim 3$, thereby allowing their comparison with galaxies at lower redshifts and in the local universe. We specifically seek to investigate the relationships between all relevant quantities, including redshift, asymmetry, concentration, size, bolometric luminosity, and star formation rate, using measurements from the combined WFPC2 and NICMOS images of the field. Such an analysis will in principle place more comprehensive constraints on models of galaxy formation and evolution than are currently available, modulo the limitations inherent in the small area of the HDF-N. We additionally include in some of our comparisons measurements made for nearby galaxies, in order to extend our analysis to the current cosmological epoch. Our approach is similar to that successfully applied in studies of quasar spectra (e.g., Boroson & Green 1992; Corbin & Boroson 1996), i.e., we test each measured quantity for correlation with every other quantity and apply a principal component analysis to the resulting correlation matrix as a means of establishing the dominant sources of variance in the sample. In the following section we describe our data and measurements. In § 3 we present the results of our statistical analysis and conclude with a discussion of them in § 4. All redshift-dependent quantities have been scaled to a cosmology of $H_0 = 65$ km s^{-1} Mpc^{-1}, $\Omega_M = 0.3$, and $\Omega_\Lambda = 0.7$.

2. DATA AND MEASUREMENTS

Our analysis is based on the final HDF-N WFPC2 images of Williams et al. (1996) and the NICMOS images of Thompson et al. (1999, hereafter T99) and D99, the latter retrieved from the *HST* archive and calibrated in the same way as the T99 images. All images have been dithered and drizzled as described in Williams et al. (1996) and T99. The D99 NICMOS images cover the same area as the WFPC2 images, while the T99 images consist of a single NICMOS camera 3 field, covering approximately one-fifth of the total WFPC2 area. The T99 images go slightly deeper than the D99 images and so were used in the area in which these images overlap.

2.1. Luminosities, Star Formation Rates, and Related Quantities

TWSL01 have used the T99 images in combination with the portion of the WFPC2 images that they overlap to measure galaxy fluxes (when possible) in each of the six associated filters (F300W, F450W, F606W, and F814W of WFPC2 and F110W and F160W of NICMOS, the latter centered at 1.1 and 1.6 μm). The addition of the NICMOS fluxes greatly improves constraints on the galaxy spectral energy distributions (SEDs). TWSL01 have used these new SEDs to measure the object photometric redshifts, bolometric luminosities, and star formation rates using a detailed galaxy spectral template fitting procedure. This procedure uses an array of galaxy SED templates that cover a range from very actively star-forming objects to objects dominated by evolved stellar populations. Specifically, starting from a basic set of six templates derived from Coleman, Wu, & Weedman (1980), Calzetti, Kinney, & Storchi-Bergman (1994), and the 1996 version of the Bruzual & Charlot (1993) SED library, TWSL01 apply the galaxy dust extinction law of Calzetti et al. (1994) for

various amounts of extinction to create an effective array of 51 templates covering a wide range of star formation rates and internal extinctions. A correction for intergalactic extinction to the redshifted templates using the formulation of Madau et al. (1996) is also included. These SEDs are then fitted to the galaxy flux points using a χ^2 procedure to estimate the object redshift. This redshift value is then used to measure the bolometric luminosity by integrating the rest-frame SED of the best-fitting template, after adding back the amount of flux estimated to be lost as a result of dust extinction. TWSL01 also estimate the fraction of the bolometric luminosity that is reradiated at 850 μm from the extinction value of the best-fitting template. The star formation rate is estimated from the unextincted flux at the rest-frame wavelength of 1500 Å using the relation of Madau, Pozzetti, & Dickinson (1998). Support for the TWSL01 SED fitting method is provided by the close agreement between their photometric redshift values of the HDF-N galaxies and those obtained spectroscopically (see their Fig. 3).

We include all these measurements (photometric redshift, bolometric luminosity, star formation rate, and fractional reemission, denoted as " Fraction ") in our analysis. We also measure the ratio of star formation rate to bolometric luminosity as an additional parameter, given the evidence that the ratio of star formation rate to galaxy mass (often called specific star formation rate) shows a strong inverse correlation with galaxy mass (Guzmán et al. 1997; Brinchmann & Ellis 2000). This correlation suggests that the ratio of star formation rate to bolometric luminosity is also of diagnostic importance. The TWSL01 measurements are for 276 objects in the T99 NICMOS image of the HDF-N; the D99 images are not included in this analysis. For the galaxies covered by the D99 images, we use the photometric redshifts in the current on-line version of the catalog[1] of Fernández-Soto, Lanzetta, & Yahil (1999), which are based on combined WFPC2 fluxes and near-infrared fluxes obtained from ground-based observations. For all objects for which spectroscopic redshifts are available in the Fernández-Soto et al. (1999) catalog, these redshifts have been used in place of the photometric redshifts.

2.2. Morphological Parameters and Sizes

We attempt to quantify the galaxy morphologies using the asymmetry and concentration parameters of Conselice, Bershady, & Jangren (2000, hereafter CBJ00) and Bershady, Jangren, & Conselice (2000). The validity of measuring these parameters for high-redshift galaxies in WFPC2 and NICMOS images is discussed by CBJ00. Briefly, based on CCD images of the local galaxy sample of Frei et al. (1996), CBJ00 find that asymmetry measurements are not strongly affected by decreases in angular resolution until a resolution limit ~ 1 h_{75}^{-1} kpc, at which point they sharply decrease relative to their initial value (see their Fig. 19). The resolution of the drizzled WFPC2 images (approximately 0″.04 pixel^{-1}) is higher than this for the adopted cosmology up to $z \cong 2$, while that of the drizzled NICMOS images (approximately 0″.1 pixel^{-1}) matches this limit more critically for the same redshift range. Thus, there should not exist any strong systematic errors in the asymmetry measurements of galaxies in either the WFPC2 or NICMOS

---

[1] See http://bat.phys.unsw.edu.au/~fsoto/hdfcat.html.

images, although we return to further discussion of this point in later sections.

The concentration parameter was first defined by Kent (1985), and a similar asymmetry parameter has been used by Abraham et al. (1996a, 1996b). These parameters are defined as

$$A \equiv \frac{\Sigma \, |(I_0 - I_{180})|}{2\Sigma \, |(I_0)|} \, ,$$

$$C \equiv 5 \, \log \left[\frac{r(80\%)}{r(20\%)} \right] .$$

I_0 and I_{180} represent the galaxy intensity per pixel after rotations of $0°$ and $180°$ from its original position. The value of this parameter ranges from 0 for a perfectly symmetric object to 1 for a completely asymmetric object. The percentages in the definition of the concentration parameter represent the fraction of the total intensity enclosed at the given radius. The measurements of both parameters include a correction for sky background and were made interactively for each galaxy using an IDL-based image display and measurement program, using an adaptation of the measurement algorithm of CBJ00. Specifically, the sky background was taken as the mode of the counts in a rectangular annulus surrounding the target galaxy. The area of this annulus was adjusted to have several times the area of the target galaxy and placed to exclude bright nearby neighbors. This background measurement differs from that used by CBJ00 involving the rotation of the background area but was found to be more practical as a result of the crowded nature of the HDF-N and its exceptionally low background noise. Each galaxy was measured 3–7 times, with the final values taken as the median of the separate trials, and galaxies with greater than 20% variance in the trial values were excluded.

These morphological parameters were chosen for several reasons. First, CBJ00 and Bershady et al. (2000) find that they are closely related to, and more quantitatively constrain, traditional classification systems such as Hubble type. They are also sensitive indicators of dynamically disturbed systems (CBJ00; Conselice, Bershady, & Gallagher 2000; see also Corbin 2000). Finally, by measuring them, we can combine our data with those of CBJ00, who measure these parameters for 113 bright nearby galaxies that roughly span the full Hubble sequence, using the deep CCD images of Frei et al. (1996). The inclusion of these data thus effectively extends our analysis of the HDF-N to the local universe.

The $(1 + z)^4$ surface brightness dimming of high-redshift galaxies will strongly affect their apparent morphologies, so any attempt to measure them must account for this effect. Our asymmetry and concentration values are thus measured at a "metric" radius derived from the curve of growth of the galaxy brightness profile, as opposed to measuring them at a fixed isophote. This is the same method used by CBJ00 and is based on the parameterization first introduced by Petrosian (1976). Specifically, under the parameterization of the galaxy intensity profile $\eta(r) \equiv I(r)/\langle I(r) \rangle$, where r is the radial distance from the galaxy center and $\langle I(r) \rangle$ is the mean intensity interior to it, CBJ00 measure their asymmetry parameters at radii corresponding to $\eta = 0.8, 0.5,$ and 0.2. Given the much smaller angular size of the HDF-N galaxies, we chose to measure their asymmetries and concentrations at only the largest radius, corre-

sponding to $\eta = 0.2$. This turned out to introduce the largest restriction on the objects for which the asymmetry and concentration could be measured, i.e., excluding over two-thirds of the galaxies in the field because the $\eta = 0.2$ radius could not be reached. However, as will be discussed in more detail in § 2.4, this did not only eliminate galaxies with small angular sizes and thereby introduce a selection effect. Rather, many of the brighter and larger galaxies in the field could not be measured to their $\eta = 0.2$ radii because of blending with neighbors. We are able to measure the rest-frame ultraviolet morphological parameters for a total of 105 galaxies and the rest-frame visible parameters for a total of 124 galaxies. The automatic object detection and measurement programs used by Williams et al. (1996), T99, and TWSL01, namely, Faint Object Classification and Analysis System (FOCAS) and SExtractor, include many objects excluded by the $\eta = 0.2$ criterion, as they also include algorithms for object deblending. In addition to the $\eta = 0.2$ criterion, our measurements of the galaxy morphological parameters are restricted to galaxies detected at signal-to-noise ratio (S/N) levels greater than 5, with a corresponding random error in the asymmetry and concentration measurements of less than 20%. Because of the exceptionally low background levels in the images, most of the galaxies are detected at this S/N level.

Inspection of the galaxies in each of the individual WFPC2 and NICMOS filter images reveals that their morphologies do not vary strongly between adjacent filters. Before measuring the galaxy asymmetries and concentrations, we therefore decided to add together the images in adjacent filters to create a set of three images having higher S/N levels. Specifically, we formed the (F300W + F450W), (F606W + F814W), and (F110W + F160W) images after first aligning the images in the separate filters to within 0.1 pixel using the centroids of stars within them. The three resulting images have effective (transmission-weighted) central wavelengths of approximately 4167 Å, 6940 Å, and 1.35 μm, respectively. We measured the asymmetry and concentration of each galaxy in each of the three images whenever possible, using the catalog lists of Williams et al. (1996) and T99 to identify objects. Using the object redshift, we then determined whether these measurements covered the rest-frame ultraviolet or rest-frame visible emission of the galaxy. This was based on whether the rest-frame 4000 Å emission of the galaxy fell below or above the image central wavelength. The rest-frame UV morphology and rest-frame visible morphology of objects at $0 < z < 0.74$ are thus measured from the (F300W + F450W) and (F606W + F814W) images, respectively, while for objects at $0.75 < z < 2.38$ they are measured from the (F606W + F814W) and (F110W + F160W) images. The rest-frame UV morphology of objects at $z > 2.38$ is covered by the (F110W + F160W) images, while their rest-frame visible emission is redshifted out of the available passbands. The choice of 4000 Å as a dividing point between UV and visible emission is arbitrary but is based on the galaxy population synthesis models of Bruzual & Charlot (1993), which show that the shape of galaxy spectra below this approximate wavelength varies most strongly with galaxy age, and the associated presence of OB stars. The rest-frame emission of a given galaxy above 4000 Å is thus most likely to trace its evolved stars and underlying mass distribution.

We find good agreement between our asymmetry and concentration measurements and the qualitative appear-

ance of the galaxies, in both the WFPC2 and NICMOS images. Examples are shown in Figure 1, which shows both the rest-frame visible images of four galaxies (extending from $z \cong 0.1$ to 2.3) and their associated brightness profiles, as traced along their major axes. The increase in the values of A(Vis), in particular, matches the progression of the asymmetries evident in the brightness profiles. This provides confidence that the asymmetry parameter measures the underlying structure of the galaxies.

2.3. Combined Measurements

In Table 1 we present the measurements used in our statistical analysis, for the objects for which morphologies could be measured. The star formation rates, bolometric luminosities, and fractional luminosities of additional objects can be found in TWSL01. The objects are identified by their names in the Williams et al. (1996) catalog and have been sorted in order of increasing right ascension. Further discussion of errors and inclusion criteria is presented in the following section. We note that the bolometric luminosity values of TWSL01 and the luminosity-normalized star formation rates we formed from them have been scaled to our adopted cosmology. We also include a measurement of object size, taken from Williams et al. (1996), for all objects for which the $\eta = 0.2$ radius could be reached. Specifically, we use their intensity-weighted first-moment radius measured from the (F606W + F814W) image and convert this to kiloparsecs. While this is the most robust measure of object size available, it should be treated with the greatest caution of all the measured parameters because of the uncertainty introduced by the variance in the object asymmetries and concentrations. Finally, for each object we note which of the four galaxy spectral templates (E, Sbc, Scd, and Irr) used by Fernández-Soto et al. (1999) was found to best fit its SED.

2.4. Errors, Biases, and Selection Effects

Despite the good motivations for combining the WFPC2 and NICMOS HDF-N images and Frei et al. (1996) local galaxy images for measuring morphological parameters, they form a heterogeneous data set, mainly in terms of image resolution. Measurements of them may thus be subject to systematic errors. To estimate these errors and to assess the validity of combining the CBJ00 measurements with our own, we performed the following tests. First, since our algorithm for the measurement of asymmetry and concentration differs slightly from that of CBJ00 in terms of the image background, we independently measured the asymmetries and concentrations of a random subset of galaxies in the Frei et al. (1996) images and found agreement between our values and those of CBJ00 to within $\sim 20\%$. As in the case of our measurements, there is also good agreement between the values of the asymmetry and concentration parameters measured by CBJ00 and Bershady et al. (2000) and the qualitative appearance of the galaxies, which further supports the combination of those measurements with our own. Concerning the WFPC2 and NICMOS images, since they differ in angular resolution by a factor of approximately 2, we tested for any systematic effect caused by this difference by resampling the WFPC2 images to the resolution of the NICMOS images and comparing the corresponding asymmetry and concentration measurements for a sample of approximately 15 randomly selected galaxies. We find no strong systematic differences in these mea-

surements, although we confirm the result of CBJ00 and Wu, Faber, & Lauer (1997) that the asymmetry values of elliptical galaxies tend to *increase* slightly as image resolution is lowered. The mean difference between the morphological parameters measured from the original and resampled WFPC2 images is approximately 20%. This indicates a source of uncertainty in the combined set of WFPC2 and NICMOS morphological measurements in addition to the relatively low errors introduced by Poisson noise in the galaxies and image background (§ 2.2). We thus estimate total random errors for the combined set of CBJ00, WPFC2, and NICMOS asymmetry and concentration parameters to be relatively large, in the range $\sim 10\%$–30%. A detailed analysis (including Monte Carlo simulations) of the possible errors in the galaxy bolometric luminosities and star formation rates is presented by TWSL01. In particular, they address the issue of the degeneracy in SEDs produced by dust extinction versus the age of the stellar population and how this affects their estimates of star formation rates and bolometric luminosities.

The Frei et al. (1996) galaxy sample is not complete in any sense, and so the combination of the morphological measurements of CBJ00 and Bershady et al. (2000) with those from the HDF-N galaxies must be carefully considered. In particular, the Frei et al. (1996) sample contains only a few dwarf irregular galaxies. However, independent of the issue of how well the local galaxy population is in fact characterized, it can be said that the Frei et al. (1996) sample covers the full range of Hubble types without a strong bias toward any one part of the sequence (see Frei et al. 1996 and CBJ00). This sample also contains several strongly asymmetric galaxies such as Arp 18 (NGC 4088) and NGC 4731, which may have recently undergone mergers. The Frei et al. (1996) sample is therefore not biased toward symmetric galaxies, which is important insofar as such a bias could create a false correlation between redshift and asymmetry when measurements of these galaxies are combined with those of galaxies in the HDF-N. We thus proceed under the assumption that the Frei et al. (1996) sample is, to first order, representative of the local galaxy population. The lack of low-luminosity irregular galaxies in this sample may in fact be beneficial for the present comparison, since this will tend to compensate for any selection against such objects at high redshift, although, as we discuss below, we find no strong evidence of incompleteness in the HDF-N sample.

As noted above, the exclusion of objects in the HDF-N for which the $\eta = 0.2$ radius could not be reached would seem to introduce a bias against very high redshift, intrinsically compact and low surface brightness galaxies. However, in practice an equally important factor in whether this radius could be reached is to what degree the galaxy is isolated. The $\eta = 0.2$ radius reaches close to the outer edges of the disks of normal spiral galaxies (see CBJ00). Consequently, many of the apparently larger galaxies in the field could not be measured to $\eta = 0.2$ because of blending with nearby objects. This also affected smaller and fainter objects. The range of bolometric luminosities over which we are able to measure asymmetries and concentrations still extends over approximately 3.3 dex, which argues against a strong luminosity bias in the sample. To assess this more quantitatively, we performed the two-sided Kolmogorov-Smirnov test on the bolometric luminosity distributions of objects for which A(Vis) could and could not be measured. We find that these distributions differ at only the 82% con-

(a)

4-916.0   4-558.0

3-430.1   4-660.0

(b)

4-916.0

A(Vis) = 0.124
C(Vis) = 3.75

4-558.0

A(Vis) = 0.311
C(Vis) = 2.67

3-430.1

A(Vis) = 0.683
C(Vis) = 4.69

4-660.0

A(Vis) = 0.801
C(Vis) = 3.73
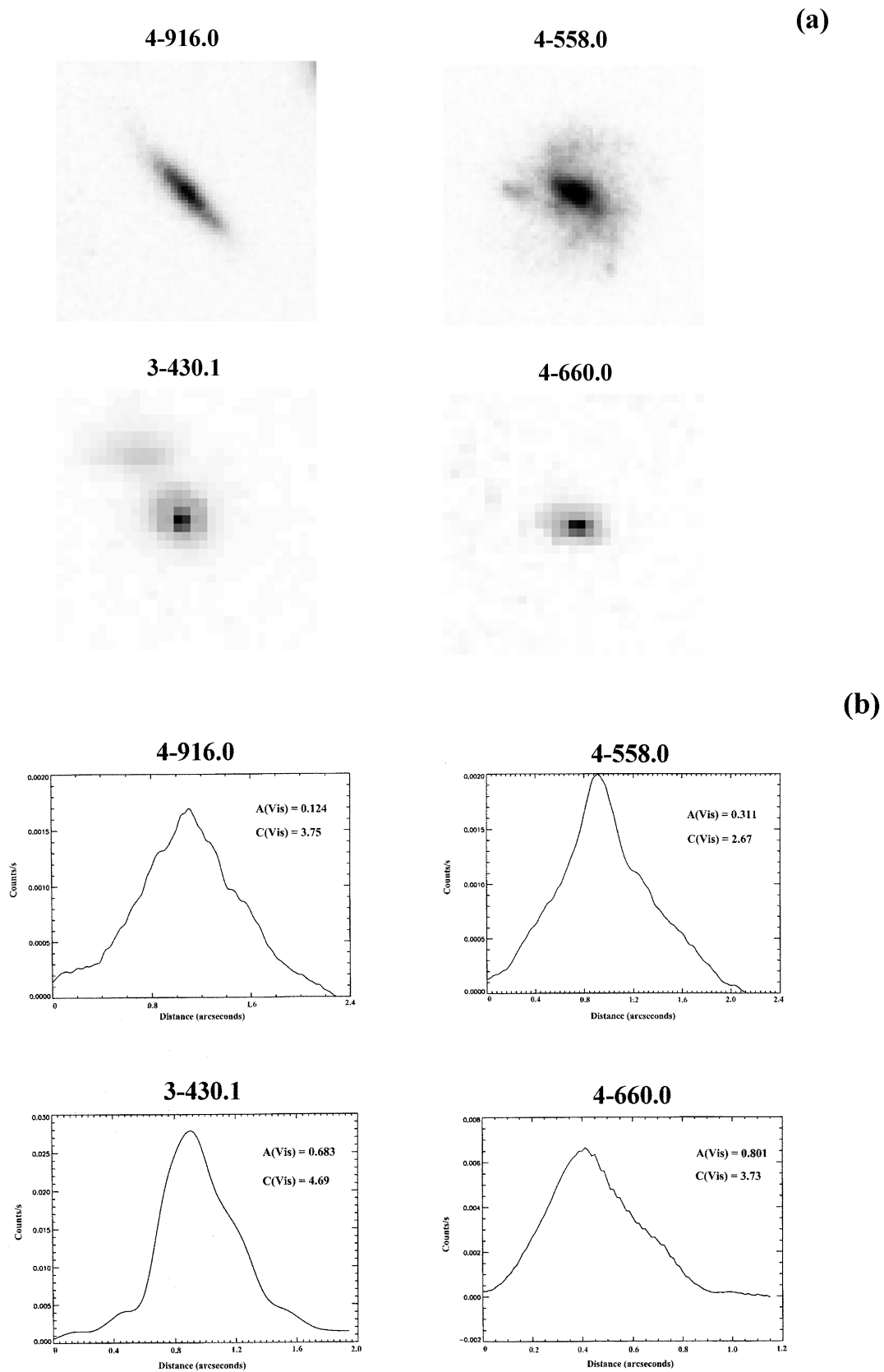
FIG. 1.—Sample galaxies from the HDF-N illustrating the range in morphological asymmetries. (*a*) Images covering the rest-frame visible emission of the galaxies 4-916.0 ($z = 0.16$), 4-558.0 ($z = 0.48$), 3-430.1 ($z = 1.231$), and 4-660.0 ($z = 2.32$). The images are 3 arcsec square. The first two galaxies are shown in the WFPC2 (F606W + F814W) image, while the last two galaxies are shown in the NICMOS (F110W + F160W) image. (*b*) Brightness profiles of the galaxies in these images, averaged over 2–5 pixels along their major axes, along with their measured asymmetry and concentration parameter values. Note the correspondence of the values of the asymmetry parameter to the appearance of the brightness profiles.

TABLE 1

Measured Parameters for HDF-N Galaxies

ID	z	r_1	A(UV)	C(UV)	A(Vis)	C(Vis)	SFR	log L_{bol}	log (SFR/L)	Fraction	Spectral Type
4-916.0......	0.16	1.0	...	...	0.124	3.75	...	...	...	...	3
4-950.0......	0.609	3.1	0.529	2.19	0.408	2.62	...	...	...	...	3
4-942.0......	1.00	1.4	0.159	3.91	0.311	4.47	...	...	...	...	2
4-823.0......	0.64	1.4	...	...	0.152	3.69	...	...	...	...	3
4-801.0......	0.92	1.5	0.467	3.70	0.482	4.37	...	...	...	...	4
4-928.0......	1.015	2.3	0.166	3.87	...	...	...	...	...	...	2
4-888.0......	1.01	1.1	0.505	2.85	...	...	...	...	...	...	4
4-878.0......	0.00:	...	0.573	3.75	0.379	3.95	...	...	...	...	2
4-822.0......	0.16	0.8	...	...	0.367	3.13	0.615	10.15	−10.36	0.95	3
4-948.0......	0.585	6.7	...	...	0.155	3.42	...	...	...	...	2
4-767.0......	0.72	1.6	...	...	0.135	4.16	0.019	10.97	−12.70	−0.02	1
4-794.0......	0.80	1.2	0.770	2.86	...	...	0.432	10.11	−10.47	0.47	4
4-976.1......	0.089	1.8	...	...	0.297	2.82	...	...	...	...	4
4-661.0......	0.52	1.0	...	...	0.170	3.73	...	...	...	...	3
4-639.1......	0.00:	...	0.684	3.86	0.473	4.06	...	...	...	...	4
4-795.0......	0.40	2.6	...	...	0.129	2.65	0.460	10.90	−11.24	0.23	3
4-665.0......	1.44	3.1	...	...	0.102	4.75	3.602	11.01	−10.45	0.60	4
4-769.0......	0.96	1.6	0.285	2.73	0.540	3.45	1.362	10.53	−10.40	0.55	4
4-671.0......	0.96	1.2	...	...	0.339	4.22	1.556	10.63	−10.44	0.75	4
4-690.0......	1.12	1.1	...	...	0.148	4.54	2.459	10.78	−10.39	0.88	4
4-602.0......	2.04	1.1	0.162	4.06	...	...	...	...	...	...	4
4-619.0......	2.96	0.8	0.762	3.84	...	...	1.219	10.69	−10.61	0.42	4
4-636.0......	0.64	0.9	...	...	...	...	1.675	10.66	−10.44	0.88	4
4-725.0......	1.84	1.6	...	...	0.288	3.59	0.661	10.38	−10.56	0.00	4
4-581.0......	1.92	1.3	...	...	...	...	6.356	11.22	−10.42	0.50	4
4-697.0......	2.48	1.1	0.166	4.18	...	...	1.818	10.78	−10.52	0.12	4
4-656.0......	0.56	3.5	0.499	2.14	0.196	2.12	67.57	12.22	−10.39	0.91	3
4-660.0......	2.32	1.4	0.613	3.55	0.801	3.73	3.257	10.93	−10.42	0.13	4
4-554.1......	0.84	1.5	0.271	3.6	...	...	...	...	...	...	4
4-493.0......	0.847	2.4	...	...	0.221	4.98	...	...	...	...	1
4-775.0......	1.12	3.4	0.309	3.04	0.204	3.67	...	...	...	...	2
4-590.0......	2.08	1.3	...	...	0.144	4.24	21.32	11.74	−10.41	0.79	4
4-727.0......	1.242	1.7	0.140	3.21	0.337	4.20	...	...	...	...	4
4-565.0......	0.56	2.0	0.286	3.11	0.207	3.06	21.52	11.72	−10.39	0.86	3
4-572.0......	0.48	1.7	...	...	...	...	1.051	10.34	−10.32	0.75	4
4-479.0......	1.12	1.1	0.393	3.94	...	...	1.512	10.61	−10.43	0.35	4
4-744.0......	0.764	3.3	...	...	0.178	4.68	...	...	...	...	1
4-439.1......	4.32	0.9	0.180	3.11	...	...	...	...	...	...	4
4-402.3......	0.557	2.9	0.344	2.22	0.176	2.41	...	...	...	...	2
2-82.1	2.267	1.8	0.756	3.91	...	...	...	...	...	...	4
1-54.2	2.929	2.1	...	...	...	...	...	...	...	...	4
4-500.0......	1.28	1.3	...	...	0.677	3.21	0.055	9.51	−10.77	0.00	4
4-430.0......	0.72	2.9	0.748	2.98	0.488	2.20	0.870	10.46	−10.52	0.26	4
4-402.0......	0.558	10.7	0.668	3.21	0.419	2.89	...	...	...	...	4
4-752.1......	1.013	4.5	0.119	3.58	...	...	...	...	...	...	1
4-627.0......	0.16	0.6	...	...	...	...	0.170	9.59	−10.36	0.95	4
4-505.1......	1.28	3.2	...	...	0.122	3.15	18.83	11.60	−10.32	0.87	2
4-527.0......	0.96	1.1	...	...	0.505	4.08	0.658	10.16	−10.32	0.88	3
4-445.0......	1.84	2.1	0.34	3.40	0.239	4.25	80.45	12.29	−10.38	0.75	4
4-579.0......	0.48	1.1	0.299	3.96	0.204	3.53	1.103	10.52	−10.48	0.56	4
4-603.0......	2.56	1.4	0.694	3.91	...	...	2.072	10.73	−10.42	0.12	4
4-558.0......	0.48	2.8	...	...	0.311	2.67	5.404	11.05	−10.32	0.84	3
4-509.0......	1.12	1.2	...	...	0.599	4.37	0.20	9.59	−11.29	0.00	...
4-351.0......	2.48	0.9	...	...	...	...	0.626	10.37	−10.57	0.11	4
4-378.0......	1.12	3.8	...	...	0.370	2.72	0.499	10.46	−10.77	0.07	4
4-596.0......	0.48	1.0	...	...	0.837	3.25	0.126	9.58	−10.48	0.23	4
4-316.0......	1.76	4.0	0.484	2.97	...	...	...	...	...	...	4
4-571.0......	0.72	2.1	0.546	2.60	0.370	2.64	0.503	10.25	−10.55	0.32	4
4-543.0......	1.28	1.8	0.983	3.26	0.817	3.93	5.356	11.08	−10.35	0.60	4
4-502.0......	2.00	2.0	...	...	0.477	3.10	7.019	11.14	−10.29	0.50	4
4-593.0......	0.40	0.0	...	...	0.220	2.83	0.781	10.33	−10.44	0.92	3
4-407.0......	0.56	1.5	...	...	0.533	3.66	2.548	10.77	−10.36	0.88	4
4-498.0......	1.92	1.1	0.646	3.4	0.608	4.45	1.694	10.74	−10.51	0.46	4
4-395.0......	0.72	1.0	...	...	0.58	3.04	1.285	10.52	−10.41	0.60	4
4-555.1......	3.12	3.8	0.19	4.46	...	...	15.28	11.81	−10.63	0.00	4

TABLE 1—*Continued*

ID	z	r_1	A(UV)	C(UV)	A(Vis)	C(Vis)	SFR	log L_{bol}	log (SFR/L)	Fraction	Spectral Type
4-368.0......	1.92	1.8	...	...	0.386	3.85	17.11	11.61	−10.38	0.73	3
4-557.0......	2.16	1.6	0.273	3.60	0.503	4.43	1.365	10.97	−10.84	0.00	4
4-344.0......	1.20	1.0	...	...	0.590	3.85	1.659	10.61	−10.39	0.58	4
4-345.0......	1.36	1.0	...	...	0.310	4.65	1.870	10.73	−10.46	0.56	4
4-389.0......	2.72	1.1	...	...	...	...	4.874	11.06	−10.37	0.42	4
4-516.0......	1.04	1.6	0.532	4.19	0.239	4.52	1.329	11.00	−10.88	0.31	3
4-307.0......	1.60	2.1	...	...	0.267	4.36	534.70	131.13	−10.40	0.97	1
4-563.0......	4.40	1.4	0.354	4.57	...	...	2.847	11.40	−10.95	0.17	2
4-497.0......	2.16	1.0	0.340	3.81	...	...	...	...	...	...	4
2-239.0......	2.427	4.3	...	...	...	...	...	...	...	...	4
4-473.0......	5.52	0.6	0.496	4.35	...	...	4.507	11.00	−10.35	0.00	4
4-305.0......	0.96	1.6	0.285	3.31	0.683	3.89	4.937	11.06	−10.37	0.88	3
4-460.0......	0.56	2.0	...	...	0.252	2.80	7.682	11.23	−10.35	0.86	4
4-254.0......	0.60	2.2	0.333	3.20	...	...	...	...	...	...	1
4-522.0......	1.12	1.4	...	...	...	...	7.191	11.23	−10.38	0.79	4
4-550.0......	1.04	5.5	0.817	2.02	0.209	2.77	1.250	11.43	−11.33	0.17	3
4-448.0......	0.48	2.2	...	...	0.451	2.82	3.561	10.82	−10.27	0.92	3
4-300.0......	0.56	1.4	0.926	3.19	...	...	1.424	10.60	−10.45	0.73	3
2-251.0......	0.96	3.0	0.184	4.75	0.105	4.96	...	...	...	...	2
4-327.0......	1.84	1.3	0.915	2.90	0.552	3.96	9.414	11.35	−10.38	0.79	4
4-303.0......	1.92	0.9	...	...	0.605	4.53	1.606	10.65	−10.44	0.69	...
2-270.0......	0.16	1.0	0.225	3.94	0.200	3.97	...	...	...	...	4
4-471.0......	0.32	1.6	...	...	...	...	0.009	10.48	−12.53	0.00	1
4-161.0......	0.92	1.7	0.103	3.25	...	...	...	...	...	...	4
4-488.0......	2.48	1.1	0.976	5.18	...	...	3.169	10.92	−10.42	0.14	4
4-416.0......	0.454	1.4	...	...	0.209	3.48	3.081	10.91	−10.42	0.77	4
4-434.0......	0.16	0.6	0.909	4.04	...	...	0.227	9.77	−10.42	0.88	4
4-350.0......	1.20	1.1	0.127	3.94	0.20	4.50	0.079	9.85	−10.95	0.00	4
4-475.0......	3.68	0.8	...	...	...	...	3.183	10.95	−10.45	0.12	4
4-442.0......	0.64	1.4	...	...	0.383	3.01	0.232	10.02	−10.65	0.38	4
4-241.0......	0.48	9.4	...	...	0.247	4.33	...	...	...	...	4
4-474.0......	1.059	6.1	...	...	0.493	2.68	...	...	...	...	4
4-382.0......	0.08	0.5	0.121	3.10	0.149	3.01	0.269	9.78	−10.35	0.95	3
4-289.0......	2.88	1.4	...	...	...	...	6.719	11.23	−10.40	0.00	4
4-241.1......	0.321	2.0	0.494	4.03	...	...	...	...	...	...	4
4-415.0......	0.48	1.3	0.348	3.93	0.742	2.60	0.460	10.08	−10.42	0.56	4
4-332.0......	0.48	1.4	...	...	0.610	3.34	1.440	10.57	−10.41	0.58	4
2-353.0......	0.609	1.5	...	...	0.189	3.07	...	...	...	...	2
2-201.0......	1.16	1.6	0.43	4.86	...	...	...	...	...	...	4
4-385.0......	0.16	0.6	...	...	...	...	0.167	9.63	−10.41	0.88	4
4-232.0......	0.40	2.6	...	...	...	...	7.773	11.23	−10.34	0.86	4
4-298.0......	2.64	1.1	...	...	...	...	1.804	10.67	−10.42	0.27	4
4-319.0......	0.72	1.3	...	...	0.683	2.69	1.988	10.68	−10.38	0.88	4
4-346.0......	0.72	2.0	...	...	...	...	0.396	10.19	−10.59	0.18	4
4-89.0	0.681	2.4	...	...	0.567	3.43	...	...	...	...	4
4-173.0......	0.929	2.0	0.171	2.70	...	...	...	...	...	...	3
4-212.0......	1.12	1.7	...	...	0.475	4.08	0.963	10.42	−10.44	0.33	4
4-304.0......	0.72	0.9	...	...	0.947	3.72	1.385	10.61	−10.47	0.91	3
2-121.0......	0.475	3.4	...	...	0.087	4.35	...	...	...	...	1
2-454.0......	2.04	2.0	0.334	4.15	0.409	4.15	...	...	...	...	4
2-537.0......	0.139	1.7	...	...	...	...	...	...	...	...	3
4-260.1......	0.96	5.4	0.910	2.40	...	...	...	...	...	...	3
4-257.0......	0.56	1.1	...	...	0.226	3.46	0.701	10.34	−10.50	0.53	4
2-246.0......	0.958	4.8	...	...	...	...	...	...	...	...	3
4-229.0......	0.80	1.2	0.626	3.75	0.342	4.52	1.19	10.56	−10.49	0.55	4
4-186.0......	1.84	3.6	0.455	2.84	0.650	4.32	375.20	13.08	−10.50	0.95	2
4-154.0......	0.48	1.4	...	...	...	...	0.815	10.33	−10.42	0.84	3
2-210.0......	0.749	4.1	0.387	2.12	0.519	2.52	...	...	...	...	4
3-258.0......	0.520	2.6	...	...	0.188	3.02	...	...	...	...	4
4-120.0......	0.72	2.9	...	...	...	...	1.699	10.90	−10.66	0.32	4
4-284.0......	0.961	2.5	0.290	3.11	...	...	...	...	...	...	2
4-235.0......	0.961	1.1	0.208	3.78	...	...	...	...	...	...	4
4-131.0......	0.72	1.8	...	...	0.558	3.10	3.471	10.90	−10.36	0.77	4
2-264.2......	0.478	10.7	0.212	3.97	0.087	3.67	...	...	...	...	3
2-256.0......	1.24	3.2	0.275	3.94	0.600	3.68	...	...	...	...	3
3-229.0......	0.76	1.5	0.175	3.24	...	...	...	...	...	...	3

TABLE 1—*Continued*

ID	z	r_1	A(UV)	C(UV)	A(Vis)	C(Vis)	SFR	log L_{bol}	log (SFR/L)	Fraction	Spectral Type
2-514.0	0.752	2.6	0.252	3.42	0.174	3.90	...	...	...	...	3
4-109.0	2.08	1.3	0.219	3.34	0.227	4.36	0.162	10.03	−10.82	0.00	4
3-143.0	0.477	2.1	0.589	3.15	0.250	3.09	...	...	...	...	2
4-85.1	2.72	1.3	...	...	...	...	5.961	11.26	−10.49	0.00	4
3-37.0	0.92	2.2	0.591	3.24	...	...	...	...	...	...	4
2-264.1	0.475	3.9	...	...	0.300	3.14	...	...	...	...	2
2-585.0	2.002	6.1	...	...	...	...	...	...	...	...	3
3-243.0	3.233	1.0	0.474	4.68	...	...	...	...	...	...	4
3-331.0	1.08	2.6	0.285	3.26	...	...	...	...	...	...	4
4-1.0	1.08	4.2	0.244	4.04	...	...	...	...	...	...	4
2-525.0	2.237	1.8	0.519	3.28	0.809	3.83	...	...	...	...	4
433.0	0.80	3.0	0.769	2.93	0.222	3.62	0.081	10.83	−11.92	0.00	1
3-386.1	0.474	4.0	0.665	2.93	0.478	2.66	...	...	...	...	3
3-321.0	0.678	3.3	...	...	...	...	...	...	...	...	1
2-661.0	0.816	3.5	0.603	2.89	...	...	...	...	...	...	4
3-203.0	0.319	1.6	0.576	3.57	...	...	...	...	...	...	4
3-259.0	0.56	4.3	...	...	0.564	2.34	...	...	...	...	4
2-404.0	0.199	4.0	0.482	2.43	0.352	2.59	...	...	...	...	3
3-550.1	2.775	2.0	0.389	4.03	...	...	...	...	...	...	4
2-762.0	0.44	2.3	...	...	0.366	2.93	...	...	...	...	4
3-174.0	0.089	1.9	...	...	0.641	2.82	...	...	...	...	4
3-659.1	0.299	2.0	0.485	3.37	0.306	3.09	...	...	...	...	2
2-652.1	0.557	3.5	...	...	0.352	3.34	...	...	...	...	2
2-531.0	0.96	2.0	0.188	2.30	0.170	3.41	...	...	...	...	3
2-702.0	0.557	2.7	0.318	3.59	...	...	...	...	...	...	3
3-777.1	0.456	2.6	...	...	...	...	...	...	...	...	4
3-696.0	0.401	1.1	0.198	3.37	0.184	3.30	...	...	...	...	4
2-637.0	3.368	0.9	0.282	5.55	...	...	...	...	...	...	4
2-809.0	0.498	2.5	...	...	0.398	2.54	...	...	...	...	3
2-834.0	1.72	2.0	...	...	...	...	...	...	...	...	4
3-886.0	1.24	1.4	0.768	4.03	...	...	...	...	...	...	4
2-561.2	2.489	1.1	...	...	...	...	...	...	...	...	4
2-643.0	2.991	1.3	...	...	...	...	...	...	...	...	4
3-551.0	0.559	2.5	0.761	3.34	0.277	3.24	...	...	...	...	3
2-901.1	3.181	1.5	...	...	...	...	...	...	...	...	4
2-950.0	0.517	2.3	...	...	...	...	...	...	...	...	3
3-350.1	0.642	3.9	0.435	2.35	0.272	2.69	...	...	...	...	2
2-860.0	0.849	2.9	0.278	2.54	0.302	3.10	...	...	...	...	3
2-824.0	2.419	1.4	...	...	...	...	...	...	...	...	4
3-118.1	2.232	1.2	0.227	3.78	...	...	...	...	...	...	4
3-786.0	1.60	4.0	0.713	3.19	...	...	...	...	...	...	4
3-743.0	1.64	1.4	0.387	3.41	...	...	...	...	...	...	4
3-132.0	0.56	1.7	0.202	3.12	...	...	...	...	...	...	4
2-903.0	2.233	1.4	0.550	3.14	0.366	4.16	...	...	...	...	4
3-180.2	0.280	1.2	...	...	0.224	2.97	...	...	...	...	4
3-266.0	0.72	1.3	...	...	0.180	3.89	...	...	...	...	1
3-180.0	0.37	4.8	...	...	...	...	...	...	...	...	4
2-1023.1	0.564	3.3	...	...	0.655	3.28	...	...	...	...	3
2-982.0	1.148	4.5	0.535	2.48	...	...	...	...	...	...	4
2-1018.0	0.559	2.6	...	...	0.585	3.51	...	...	...	...	4
3-486.0	0.79	3.5	0.321	3.32	0.465	3.98	...	...	...	...	3
3-443.0	0.95	5.3	...	...	...	...	...	...	...	...	4
3-512.0	4.022	1.2	0.174	3.91	...	...	...	...	...	...	4
2-906.0	1.08	2.9	...	...	0.378	3.22	...	...	...	...	4
3-943.0	0.321	1.8	...	...	0.194	2.95	...	...	...	...	3
3-815.0	0.76	2.8	0.336	4.13	0.329	4.64	...	...	...	...	1
3-430.1	1.231	1.9	...	...	0.683	4.69	...	...	...	...	2
3-610.1	0.517	6.2	...	...	...	...	...	...	...	...	2
3-355.0	1.28	2.2	...	...	0.207	4.30	...	...	...	...	2
3-404.0	0.52	4.3	0.198	2.86	...	...	...	...	...	...	3
3-773.0	0.561	3.4	...	...	0.460	2.38	...	...	...	...	4
3-400.1	0.473	4.4	0.75	3.50	...	...	...	...	...	...	4
3-221.1	0.952	4.4	...	...	0.602	2.80	...	...	...	...	4
3-405.1	0.319	2.0	0.255	3.13	0.211	3.37	...	...	...	...	4
3-957.0	1.02	1.5	0.183	3.0	0.547	3.79	...	...	...	...	4
3-863.0	0.681	1.5	...	...	0.210	2.80	...	...	...	...	4

TABLE 1—*Continued*

ID	z	r_1	A(UV)	C(UV)	A(Vis)	C(Vis)	SFR	log L_{bol}	log (SFR/L)	Fraction	Spectral Type
3-534.0......	0.32	5.0	...	...	0.192	2.69	...	...	...	...	4
3-853.1......	3.88	0.5	...	...	...	...	...	...	...	...	4
3-908.0......	0.76	5.5	...	...	...	...	...	...	...	...	4
3-958.0......	0.92	0.8	...	...	...	...	...	...	...	...	3
3-875.0......	2.04	2.8	0.643	3.12	...	...	...	...	...	...	1
3-790.1......	0.562	2.6	0.226	3.31	0.124	3.82	...	...	...	...	1

NOTE.—Identification (ID) is from the Williams et al. 1996 catalog, where numbers have been truncated to one decimal place after the primary designation; r_1 denotes the first-moment galaxy radius from Williams et al. 1996, converted to kiloparsecs. Star formation rate (SFR) is in units of $M_\odot$ yr^{-1}. Bolometric luminosity (L_{bol}) is in units of solar bolometric luminosity. The parameter "Fraction" is the fraction of the bolometric luminosity radiated in the mid- and far-infrared (see TWSL01). Spectral type is taken from Fernández-Soto et al. 1999 and is coded as follows: (1) elliptical galaxy, (2) Sbc galaxy, (3) Scd galaxy, (4) irregular galaxy. Table 1 is also available in machine-readable form in the electronic edition of the *Astrophysical Journal*.

fidence level. As the total TWSL01 sample is ~20%–30% complete compared to the local luminosity function to $z = 2$, we thus assume a similar completeness in the subsample for which A(Vis) is measured. The remaining incompleteness is likely due to excluding low surface brightness and/or low-luminosity irregular galaxies, as well as galaxies with high levels of internal extinction that consequently have reduced rest-frame UV emission (see TWSL01). As presented in the next section, we also find no correlation between redshift and galaxy size among the galaxies for which we are able to measure the morphological parameters, which argues that we have not selected against small galaxies at high redshift.

Finally, an analysis by Storrie-Lombardi, Thompson, & Weymann (1999) indicates that ~95% of the most compact objects (those having areas less than 0.2 arcsec^2) in the T99 portion of the HDF-N are likely to be at $z > 2$, which is close to the limit at which our (F110W + F160W) NICMOS images still cover the rest-frame visible continua of these galaxies. Their exclusion thus does not seriously harm our effort to trace the evolution of the rest-frame visible morphologies of these galaxies, which, as discussed previously, should be a better indicator of their underlying mass distribution. The HDF-N galaxies also show peaks in their redshift distribution, mainly at $z \simeq 0.5$ and $z \simeq 1$ (Cohen et al. 1996), which is likely the effect of large-scale structure within the pencil beam of the field. The effect of these peaks on the present analysis is unclear, but any bias may again be compensated by the fact that our morphological measurements exclude some of the apparently larger and more grouped galaxies as a result of the overlap of their brightness profiles.

3. ANALYSIS AND RESULTS

We ran the Spearman rank correlation test on all pairs of measured parameters listed in Table 1. For the comparisons involving A(Vis) and C(Vis), we include the asymmetry and concentration parameters measured by CBJ00 and Bershady et al. (2000) at the $\eta = 0.2$ radii of the R- and r-band images of Frei et al. (1996) for 113 nearby galaxies. The resulting correlation matrix is given in Table 2, which lists the Spearman rank test correlation coefficient. Values of this coefficient greater than 0.4 indicate a correlation at greater than 99% confidence, while values greater than 0.5 indicate a correlation at greater than 99.99% confidence. The number of objects involved in the individual tests varies from a maximum of 276 to a minimum of 33. The principal component analysis of this correlation matrix is presented in Table 3, which lists the coefficients of the first four eigenvectors. We consider first the results of the individual correlation tests, given the relatively few cases in which a correlation is indicated at high (greater than 99.99%) confidence.

Comparisons of the A(Vis), A(UV), C(Vis), and C(UV) measurements offer additional diagnostic tests of these parameters. These comparisons are shown in Figure 2, which shows a weak correlation in the case of the A(Vis)-A(UV) comparison and a stronger correlation between C(Vis) and C(UV). This is consistent with the qualitative findings of Bunker (1999) and D99 that there is a general agreement between the morphologies of HDF-N galaxies in the rest-frame UV and visible. Importantly, the C(Vis) values are larger on average than the corresponding C(UV) values. This is consistent with the expectation that spiral

TABLE 2

CORRELATION MATRIX

Parameter	z	r_1	A(UV)	C(UV)	A(Vis)	C(Vis)	SFR	log L_{bol}	log (SFR/L)	Fraction
z	1	−0.044	−0.010	0.351	0.557	0.211	0.520	0.500	0.155	−0.528
r_1	−0.044	1	0.088	−0.467	−0.122	−0.323	0.447	0.540	0.133	0.120
A(UV)	−0.010	0.088	1	−0.130	0.436	−0.216	0.013	0.081	0.253	0.121
C(UV)	0.351	−0.467	−0.130	1	0.029	0.630	0.017	−0.065	−0.061	−0.410
A(Vis)	0.557	−0.122	0.436	0.029	1	−0.216	−0.002	−0.221	0.135	−0.024
C(Vis)	0.211	−0.323	−0.216	0.630	−0.216	1	0.089	0.118	−0.165	−0.136
SFR	0.520	0.447	0.013	0.017	−0.002	0.089	1	0.923	0.471	0.134
log L_{bol}	0.500	0.540	0.081	−0.065	−0.221	0.118	0.923	1	0.238	0.041
log (SFR/L)......	0.155	0.133	0.253	−0.061	0.135	−0.165	0.471	0.238	1	0.329
Fraction	−0.528	0.120	0.121	−0.410	−0.024	−0.136	0.134	0.041	0.329	1

NOTE.—Values are the Spearman rank test correlation coefficient.

TABLE 3
PRINCIPAL COMPONENT ANALYSIS OF CORRELATION MATRIX

Eigenvector	z	r_1	A(UV)	C(UV)	A(Vis)	C(Vis)	SFR	$\log L_{bol}$	$\log$ (SFR/L)	Fraction
1	-0.447	0.827	0.368	-0.945	-0.164	-0.819	0.460	0.431	0.660	0.727
2	0.482	0.373	-0.665	0.139	-0.570	0.360	0.836	0.866	-0.032	-0.348
3	-0.740	-0.045	-0.415	0.014	-0.763	0.378	-0.224	-0.145	-0.199	0.485
4	-0.058	0.374	0.118	-0.184	0.006	-0.103	-0.143	0.074	-0.702	-0.190

NOTE.—Values are coefficients of the linear addition of parameter values. Eigenvalues of the individual eigenvectors are 3.97 (eigenvector 1), 2.86 (eigenvector 2), 1.79 (eigenvector 3), and 0.76 (eigenvector 4).

galaxies will appear less concentrated in the rest-frame UV, as the emission in that regime will be dominated by star-forming regions in their disks. Similarly, the A(UV) measurements are skewed to slightly higher values than the A(Vis) measurements, also consistent with having the galaxies' UV emission dominated by irregularly distributed regions of star formation (e.g., the galaxy HDF-N 4-378; see Bunker 1999). The results of Figure 2 thus provide additional confidence that the chosen wavelength dividing point between UV and visible adequately discriminates between the early- and late-type stars in these galaxies.

Several of the correlations with redshift are due to unavoidable selection effects. Specifically, the apparent correlations between redshift and bolometric luminosity, star formation rate, and mid-infrared fractional luminosity are likely due, as noted above, to the nondetection of dwarf galaxies, low surface brightness galaxies, and heavily extincted galaxies at $z > 1$. However, the strongest correlation revealed within the sample, between bolometric luminosity and star formation rate, is intrinsically meaningful. This comparison is shown in Figure 3. What is particularly noteworthy in this comparison is the clear deviation of the galaxies whose SEDs indicate that they are dominated by evolved stellar populations, as determined by TWSL01. Not surprisingly, inspection of their images reveals that

these galaxies are the most elliptical in appearance and have the reddest colors. We discuss the possible significance of this result in the next section. The strength of this correlation clearly reduces the use of the luminosity-normalized star formation rate parameter, as this ratio is thus nearly constant.

Only two other pairs of variables are correlated at greater than 99.99% confidence. The first is bolometric luminosity and galaxy radius. This is not unexpected and can be better constrained from samples of nearby galaxies. Given the related uncertainties inherent in the radius measurements (§ 2.2), this result will not be considered further. The second correlation is between redshift and A(Vis). The significance of this correlation is dependent on the inclusion of the CBJ00 asymmetry values: if this comparison is restricted to only the HDF-N galaxies, the Spearman rank test coefficient falls to 0.250. Yet as discussed above, we believe that this inclusion is valid, based in part on our ability to reproduce the CBJ00 values for the same data and the wide range of Hubble types and asymmetries covered by this sample. However, given the large uncertainties associated with the asymmetry measurements for the combined sample (§ 2.4), as well as the uncertainties in the associated photometric redshifts, the putative correlation should only be regarded as suggestive. However, it can be noted that any systematic
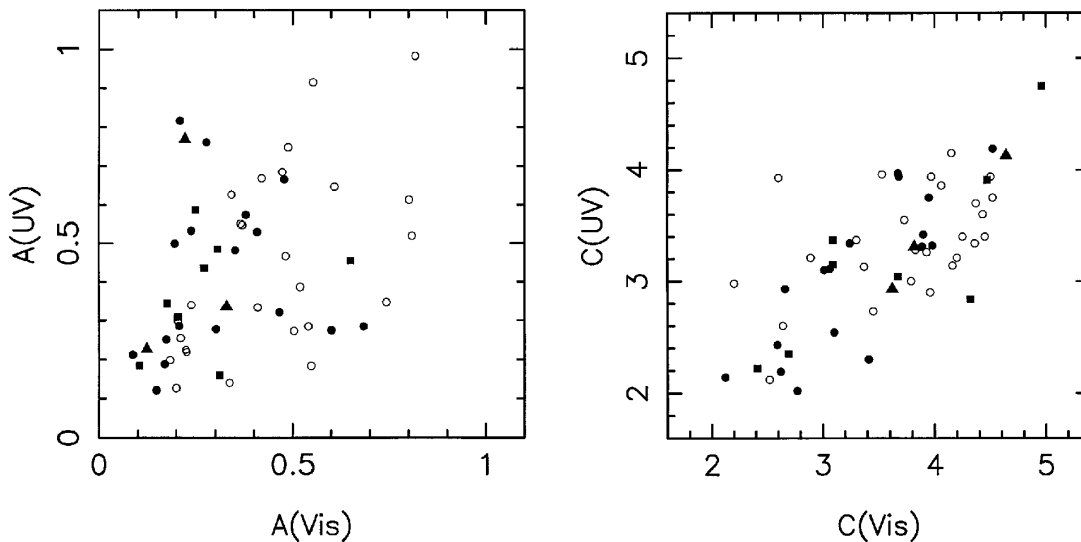
FIG. 2.—Comparison of the rest-frame ultraviolet and rest-frame visible asymmetry and concentration parameters for the sample galaxies, for each object in which both could be measured. Correlation coefficients for these comparisons are listed in Table 2. Object symbols are based on the classification of their spectral energy distributions by Fernández-Soto et al. (1999), with filled triangles denoting objects best fitted by an elliptical galaxy spectrum, filled squares denoting objects best fitted by an Sbc galaxy spectrum, filled circles denoting objects best fitted by an Scd galaxy spectrum, and open circles denoting objects best fitted by an irregular galaxy spectrum.
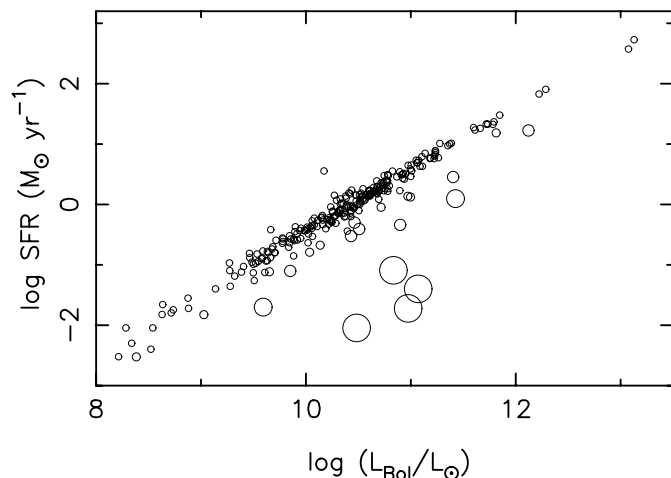
FIG. 3.—Comparison of galaxy bolometric luminosities and star formation rates. Symbol sizes are based on the set of spectral templates used by TWSL01 to fit the object spectral energy distributions. Larger circles represent galaxies best fitted by "colder" templates having lower rest-frame ultraviolet flux and older stellar populations.

bias in the asymmetry measurements of the highest redshift ($z \sim 2$) galaxies in the sample would be that their asymmetry values are *underestimated*, as this would be the result if the NICMOS images do not adequately resolve them (§ 2.2). Higher asymmetry values for these galaxies would strengthen the suggested correlation.

The comparison of redshift and A(Vis) is shown in Figure 4. In the bottom panel of Figure 4 we show the mean values of these data after binning them in redshift intervals of approximately 0.5 (the actual size of the intervals was selected to maintain subsamples of approximately equal numbers of objects, to within the irregularity in the redshift distribution). These mean values show a monotonic increase that is most clear when redshift is converted to look-back time. This is shown in Figure 5, where it can be seen that the mean asymmetry values increase by a factor of approximately 3 from the present epoch to $z \cong 2$. Two points are worth noting. First, the scatter in the comparison of the individual measurements (Figure 4, *top panel*) is obviously large, and it is possible to find galaxies as symmetric and asymmetric as those in the nearby galaxy sample at any redshift up to $z \cong 2$. However, there are no galaxies in the HDF-N that match the lower asymmetry range of the local sample. In particular, all the elliptical galaxies in the HDF-N have asymmetry values slightly above their local counterparts. This may, however, be an artifact of their higher redshifts. Specifically, as noted previously, our simulations, as well as those of CBJ00 and Wu et al. (1997), show that while the initial decrease in the angular size of disk galaxies with redshift tends to lower their asymmetry values, for elliptical galaxies the opposite (and counterintuitive) result is obtained, i.e., their asymmetries *increase* slightly as resolution is lowered. We return to further discussion of this result in the next section.

Finally, we consider the results of the principal component analysis (Table 3). The lack of a large number of correlations between the measured parameters, as well as the existence of the observationally biased correlations with redshift, makes these results of limited use. It is, however, interesting to note that the first eigenvector is dominated by
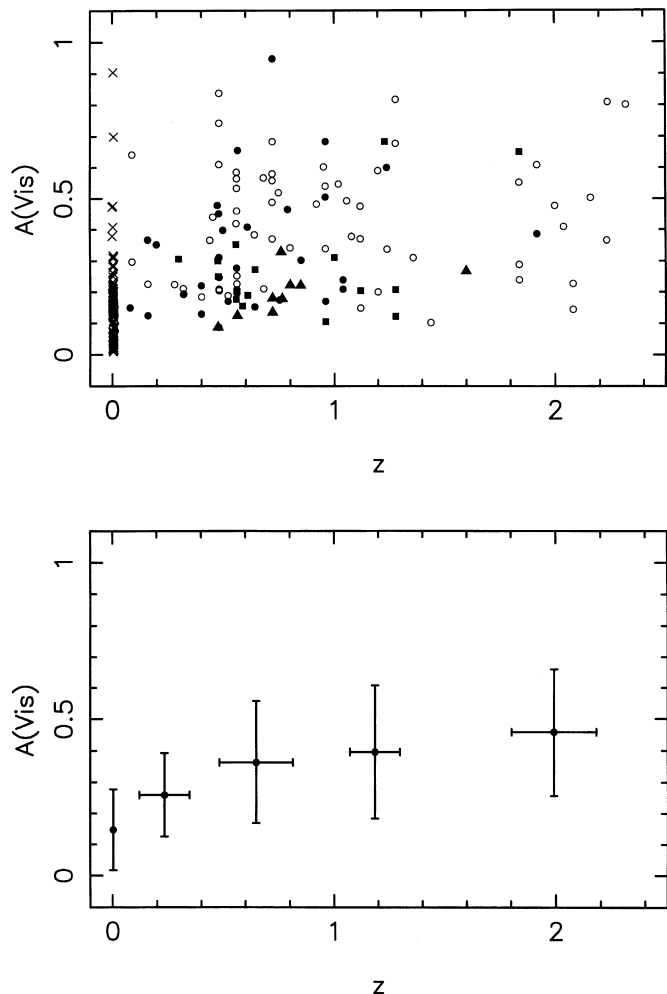
FIG. 4.—*Top:* Comparison of galaxy rest-frame visible asymmetry values and redshifts. Symbols are the same as in Fig. 2, but with crosses representing the measurements of CBJ00 for the nearby galaxy sample of Frei et al. (1996). *Bottom:* Mean values of data in top panel, binned for five subsamples of approximately equal size. Error bars represent 1 σ values of each quantity within the subsamples.

the anticorrelation of the radius and concentration parameters, although the individual correlations are not very strong (Table 2). The mid-infrared fractional luminosity and luminosity-normalized star formation rate also appear to be involved in this relation. The second and third eigenvectors are dominated by the individual correlations between bolometric luminosity and star formation rate and between redshift and A(Vis). The fourth eigenvector is most strongly related to radius and normalized star formation rate.

4. DISCUSSION

The interpretation of the one strong correlation we find, between bolometric luminosity and star formation rate, must take into account that both of these measurements are *indirect* and to first order represent quantities scaled from the fitted galaxy spectral templates. It is thus not surprising that they are correlated at some level. As discussed previously, the sample could also be slightly biased against actively star-forming but intrinsically faint galaxies such as Magellanic-type irregulars, which would weaken the correlation. However, to the extent that both quantities are accu-
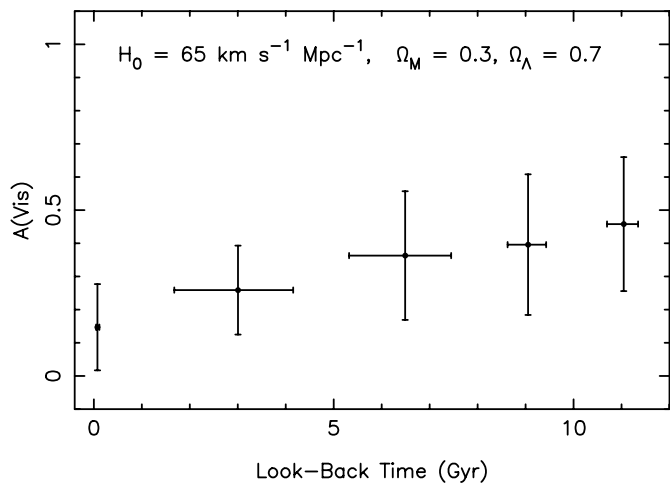
FIG. 5.—Same as Fig. 4 (*bottom panel*), but after converting redshift to look-back time under the adopted cosmology.

rately represented, this correlation shows the dominance of OB stars and active star formation on the value of bolometric luminosity. The deviation of luminous early-type galaxies from the main locus of points evident in Figure 3 thus suggests a more advanced evolutionary state for them than their late-type counterparts. This is consistent with the "downsizing" picture first introduced by Cowie et al. (1996; see also Guzmán et al. 1997; Balland, Silk, & Schaeffer 1998) in which more massive galaxies are the first to form. However, these results do not necessarily imply a monolithic collapse, as opposed to hierarchical, formation process for early-type galaxies. As noted above, the elliptical galaxies in the HDF-N are more asymmetric than their local counterparts, which may or may not be an artifact of their reduced angular size. If this effect is real, it suggests that these elliptical galaxies, which occur in the HDF-N mainly at $z < 1$ (see Fig. 4, *top panel*), are not as dynamically relaxed as elliptical galaxies in the local universe. Menanteau et al. (1999) also find evidence of lingering star formation among faint elliptical galaxies identified in archival WFPC2 images, which is inconsistent with a monolithic collapse at high redshift, and Corbin et al. (2000b) identify several galaxies in the NICMOS parallel fields that appear to be elliptical galaxies in the process of merging. A hierarchical formation process may thus apply to both disk and spheroidal galaxies, with the latter simply beginning the process earlier than the former and also more efficiently converting their gas to stars (see Balland et al. 1998).

We proceed with the interpretation of the suggested trend between redshift and rest-frame visible asymmetry under the assumption that this trend is, while weak, a real effect involving evolution in galaxy structure. If this result is spurious, then it indicates either that previous claims of galaxy morphological evolution (§ 1) are in error as a result of the lack of morphological K-corrections, or else that the chosen asymmetry parameter fails to quantify this evolution. However, in support of the view that this relation is real, we note the results of Brinchmann & Ellis (2000), who have approached this problem by making estimates of the masses of galaxies out to $z \sim 1$ and find a strong evolution in these masses for galaxies classified as peculiar or interacting.

Indeed, a direct comparison of redshift and galaxy masses provides the most fundamental test of hierarchical formation models and will be pursued with the present data in later studies. A drawback for such comparisons, however, is that the mass estimates are model dependent and subject to the array of errors inherent in the galaxy flux measurements and SED template fittings (see TWSL01). The asymmetry parameter offers a more direct measurement while not directly constraining a physical quantity. Measurement of this asymmetry parameter for the N-body simulations of galaxy formation and mergers (e.g., Walker, Mihos, & Hernquist 1996; Contardo, Steinmetz, & Fritze-von Alvensleben 1998) would be very useful as a means of matching them to these observational results.

The salient feature of the look-back time–asymmetry relation (Fig. 5) is its continuous and roughly linear form, extending through the present epoch as defined by the nearby galaxy sample. This strongly suggests that galaxy morphological evolution is a gradual process that is continuing through the present epoch, as opposed to a relatively short (~ 1–4 Gyr) formation/relaxation epoch above $z \sim 1$ followed by little or no structural changes. Several lines of evidence suggest that the "minor" mergers of large disk galaxies with smaller companions dominate this process. The first is the qualitative similarity of the N-body simulations of such mergers by Walker et al. (1996) to the appearance of many HDF-N galaxies. These simulations yield asymmetric galaxy morphologies similar to those observed (e.g., HDF-N 3-430.1 and HDF-N 4-660.0; Fig. 1a) within a period ~ 0.5 Gyr before the completion of the merger. A large number of the galaxies in the present sample, e.g., HDF-N 4-558.0 (Fig. 1a), show evidence of being in the early stage of such mergers and have small, marginally resolved companions. Walker et al. (1996) find that the effect of such mergers is to transform late-type spiral galaxies effectively into early-type spiral galaxies by enlarging the galaxy bulges upon their completion. This would account for the increase in the fraction of late-type spiral galaxies with redshift noted by both Driver et al. (1998) and Im et al. (1999) and the result of Brichmann & Ellis (2000) that morphological evolution is coupled to changes in galaxy mass. Such a model is also consistent with the evolution in the incidence of galaxy pairs (see the references in § 1), modulo the uncertainties in the relative masses of the pair members. Finally, there is ample evidence from nearby spiral galaxies that minor mergers are affecting, and will continue to affect, galaxy morphologies. First, Zaritsky et al. (1997) have found that $\sim 75\%$ of isolated spiral galaxies have at least one small nearby companion, and such companions are likely to merge with the host within the next few gigayears. Second, Zaritsky & Rix (1997) and Rudnick & Rix (1998) find that the incidence of nearby spiral galaxies in which a minor merger may have recently (within less than 1 Gyr) occurred is $\sim 20\%$–30%, as judged from the asymmetry of their disks. The continuous decrease in the mean asymmetry values seen in Figure 5 would then indicate a concurrent decrease in the galaxy merger rate with time, a conclusion also reached by Carlberg et al. (2000) and Le Fèvre et al. (2000) on the basis of the redshift dependence of the number of galaxy pairs.

This is not to say that major mergers of larger disk and spheroidal galaxies play no role in the observed morphological evolution. Indeed, TWSL01 find that two HDF-N galaxies (4-186.0 and 4-307.0) have luminosities that qualify

them as ultraluminous infrared galaxies (ULIRGs), which at low redshift show clear evidence of being major mergers (see Surace, Sanders, & Evans 2000 and references therein). ULIRGs in the range $1 < z < 2$ may comprise a significant fraction of the population of extremely red objects, which itself appears to be a significant fraction of the galaxy population in this redshift range (see Corbin et al. 2000a and references therein). However, the continuity between the asymmetry values of local galaxies not undergoing major mergers with their high-redshift counterparts (Fig. 5), along with the simple fact that most local galaxies do not appear to be the products of major mergers, suggests that minor mergers are the dominant source of the observed evolution.

Finally, we comment on the absence of correlations that we suspected, ab initio, of being present. There is no strong correlation between redshift and C(Vis) (Table 2), which could be expected under the interpretation that the trend between redshift and asymmetry is driven by merging. That is, if, as the models of Walker et al. (1996) show, minor mergers increase the bulge sizes of spiral galaxies, then before such mergers are complete, such galaxies would appear less concentrated. The lack of such a correlation could be because of the choice of the outer and inner radii used in the concentration parameter and/or could indicate a more complex relationship between morphology and minor mergers than the Walker et al. (1996) models imply. The lack of any evidence of correlation between asymmetry and star formation rate is also somewhat surprising. Le Fèvre et al. (2000) have claimed that mergers boost the star formation rates of galaxies at intermediate redshifts by a factor of roughly 2, as derived from [O II] line equivalent widths. Among nearby galaxies, Rudnick, Rix, & Kennicutt (2000) find a similar (but smaller) increase in the star formation rates of galaxies that appear recently (within the last ~ 1 Gyr) to have undergone minor mergers. A possible explanation for the lack of such a correlation among our galaxies is the evidence that the star formation of high-redshift galaxies proceeds episodically. Specifically, Sawicki & Yee (1998; see also Somerville, Primack, & Faber 2000) find that the $z > 2$ Lyman break galaxies in the HDF-N are dominated by very young (~ 25 Myr) stellar populations. Such an age is short relative to the timescale over which minor mergers produce strong asymmetries (~ 500 Myr; see Walker et al. 1996). Thus, if merging produces a series of bursts of such short duration followed by longer periods of quiescence, it would effectively remove any correlation between star formation rate and asymmetry. This could also contribute to the lack of a correlation between bolometric luminosity and luminosity-normalized star formation rate similar to that found between galaxy mass and mass-normalized star formation rate (Guzmán et al. 1997; Brinchmann & Ellis 2000). That is, given the evidence that short-lived early-type stars dominate the bolometric luminosities of these galaxies (Fig. 3), episodic star formation would serve to obscure any mass-luminosity correlation and consequently any correlations involving the luminosity-normalized star formation rate. Mass estimates of more galaxies above $z \sim 1$ will be required to test to what epochs the correlations found by Guzmán et al. (1997) and Brinchmann & Ellis (2000) extend. Alternatively, or perhaps additionally, the relation between mergers and star formation inferred among local galaxies may not apply at earlier epochs, particularly if the stellar and neutral hydrogen mass distributions of galaxies at such epochs are significantly different.

REFERENCES

Abraham, R. G., Tanvir, N. R., Santiago, B. X., Ellis, R. S., Glazebrook, K., & van den Bergh, S. 1996a, MNRAS, 279, L47
Abraham, R. G., van den Bergh, S., Glazebrook, K., Ellis, R. S., Santiago, B. X., Surma, P., & Griffiths, R. E. 1996b, ApJS, 107, 1
Balland, C., Silk, J., & Schaeffer, R. 1998, ApJ, 497, 541
Baugh, C. M., Cole, S., Frenk, C. S., & Lacey, C. G. 1998, ApJ, 498, 504
Bershady, M. A., Jangren, A., & Conselice, C. J. 2000, AJ, 119, 2645
Boroson, T. A., & Green, R. F. 1992, ApJS, 80, 109
Brinchmann, J., & Ellis, R. S. 2000, ApJ, 536, L77
Bruzual, G., & Charlot, S. 1993, ApJ, 405, 538
Bunker, A. 1999, in ASP Conf. Ser. 191, Photometric Redshifts and High-Redshift Galaxies, ed. R. J. Weymann, L. J. Storrie-Lombardi, M. Sawicki, & R. J. Brunner (San Francisco: ASP), 317
Burkey, J. M., Keel, W. C., Windhorst, R. A., & Franklin, B. E. 1994, ApJ, 429, L13
Calzetti, D., Kinney, A. L., & Storchi-Bergman, T. 1994, ApJ, 429, 582
Carlberg, R. G., et al. 2000, ApJ, 532, L1
Cohen, J. G., Cowie, L. L., Hogg, D. W., Songaila, A., Blandford, R., Hu, E. M., & Shopbell, P. 1996, ApJ, 471, L5
Coleman, G. D., Wu, C.-C., & Weedman, D. W. 1980, ApJS, 43, 393
Conselice, C. J., Bershady, M. A., & Gallagher, J. S., III 2000, A&A, in press (astro-ph/0001195)
Conselice, C. J., Bershady, M. A., & Jangren, A. 2000, ApJ, 529, 886 (CBJ00)
Contardo, G., Steimetz, M., & Fritze-von Alvensleben, U. 1998, ApJ, 507, 497
Corbin, M. R. 2000, ApJ, 536, L73
Corbin, M. R., & Boroson, T. A. 1996, ApJS, 107, 69
Corbin, M. R., O'Neil, E., Thompson, R. I., Rieke, M. J., & Schneider, G. 2000a, AJ, 120, 1209
Corbin, M. R., Vacca, W. D., O'Neil, E., Thompson, R. I., Rieke, M. J., & Schneider, G. 2000b, AJ, 119, 1062

Cowie, L. L., Songaila, A., Hu, E. M., & Cohen, J. G. 1996, AJ, 112, 839
Dickinson, M. 1999, in ASP Conf. Ser. 193, The Hy-Redshift Universe: Galaxy Formation and Evolution at High Redshift, ed. A. J. Bunker & W. van Bruegel (San Francisco: ASP), 234 (D99)
Driver, S. P., Fernández-Soto, A., Couch, W. J., Odewahn, S. C., Windhorst, R. A., Phillipps, S., Lanzetta, K., & Yahil, A. 1998, ApJ, 496, L93
Fernández-Soto, A., Lanzetta, K. M., & Yahil, A. 1999, ApJ, 513, 34
Frei, Z., Guhathakurta, P., Gunn, J. E., & Tyson, J. A. 1996, AJ, 111, 174
Glazebrook, K., Ellis, R., Santiago, B., & Griffiths, R. 1995, MNRAS, 275, L19
Guzmán, R., Gallego, J., Koo, D. C., Phillips, A. C., Lowenthal, J. D., Faber, S. M., Illingworth, G. D., & Vogt, N. P. 1997, ApJ, 489, 559
Im, M., Griffiths, R. E., Naim, A., Ratnatunga, K. U., Roche, N., Green, R. F., & Sarajedini, V. 1999, ApJ, 510, 82
Kaufmann, G., Colberg, J. M., Diaferio, A., & White, S. D. M. 1999, MNRAS, 303, 188
Kent, S. M. 1985, ApJS, 59, 115
Le Fèvre, O., et al. 2000, MNRAS, 311, 565
Madau, P., Ferguson, H. C., Dickinson, M. E., Giavalisco, M., Steidel, C. C., & Fruchter, A. 1996, MNRAS, 283, 1388
Madau, P., Pozzetti, L., & Dickinson, M. 1998, ApJ, 498, 106
Menanteau, F., Ellis, R. S., Abraham, R. G., Barger, A. J., & Cowie, L. L. 1999, MNRAS, 309, 208
Neuschaefer, L. W., Im, M., Ratnatunga, K. U., Griffiths, R. E., & Casertano, S. 1997, ApJ, 480, 59
Petrosian, V. 1976, ApJ, 209, L1
Rudnick, G., & Rix, H.-W. 1998, AJ, 116, 1163
Rudnick, G., Rix, H.-W., & Kennicutt, R. C., Jr. 2000, ApJ, 538, 569
Sawicki, M., & Yee, H. K. C. 1998, AJ, 115, 1329
Somerville, R. S., Primack, J. R., & Faber, S. M. 2000, MNRAS, in press (astro-ph/0006364)

Storrie-Lombardi, L. J., Weymann, R. J., & Thompson, R. I. 1999, in ASP Conf. Ser. 191, Photometric Redshifts and High-Redshift Galaxies, ed. R. J. Weymann, L. J. Storrie-Lombardi, M. Sawicki, & R. J. Brunner (San Francisco: ASP), 86

Surace, J. A., Sanders, D. B., & Evans, A. S. 2000, ApJ, 529, 170

Thompson, R. I., Storrie-Lombardi, L. J., Weymann, R. J., Rieke, M. J., Schneider, G., Stobie, E., & Lytle, D. 1999, AJ, 117, 17 (T99)

Thompson, R. I., Weymann, R. J., & Storrie-Lombardi, L. J. 2001, ApJ, 546, 694 (TWSL01)

van den Bergh, S., Cohen, J. G., Hogg, D. W., & Blandford, R. 2000, AJ, 120, 2190

van Dokkum, P. G., Franx, M., Fabricant, D., Kelson, D. D., & Illing-worth, G. D. 1999, ApJ, 520, L95

Walker, I. R., Mihos, J. C., & Hernquist, L. 1996, ApJ, 460, 121

Williams, R. E., et al. 1996, AJ, 112, 1335

Wu, K. L., Faber, S. M., & Lauer, T. 1997, BAAS, 191, 105.10

Zaritsky, D., & Rix, H.-W. 1997, ApJ, 477, 118

Zaritsky, D., Smith, R., Frend, C., & White, S. D. M. 1997, ApJ, 478, 39